REPORT

[OVERLINE]

Connections between groundwater flow and transpiration partitioning

Reed M. Maxwell[1] and Laura E. Condon[2]

Understanding freshwater fluxes at continental scales will help us better predict hydrologic response and manage our terrestrial water resources. The partitioning of evapotranspiration into bare soil evaporation and plant transpiration remains a key uncertainty in the terrestrial water balance. We used integrated hydrologic simulations that couple vegetation and land-energy processes with surface and subsurface hydrology, to study transpiration partitioning at the continental scale. Both latent heat flux and partitioning are connected to water table depth, and including lateral groundwater flow in the model increases transpiration partitioning from 47 ± 13% to 62 ± 12%. This suggests that lateral groundwater flow, which is generally simplified or excluded in earth system models, may provide a missing link for reconciling observations and global models of terrestrial water fluxes.

Evapotranspiration is the largest terrestrial water flux, typically accounting for more water than runoff and for about 60% of precipitation (*1*). It contributes a substantial portion of the global land-energy budget (*2*) as latent heat (*LH*) flux, which affects regional climate (*3*). Evapotranspiration commonly refers to the combination of all evaporation (*E*) from bare soil, water bodies, plant canopy, and sublimation from snow, and transpiration (*T*) through plant stoma during photosynthesis. Here we focus on the partitioning of *ET* into bare soil *E* and plant *T*. Because *T* depends on plant processes, whereas *E* depends on on shallow soil moisture and energy availability, these two factors respond differently to physical drivers and stress. Disentangling these fluxes over large scales is a key step toward improved understanding and prediction of watershed dynamics, especially when considering future stresses.

Connectivity between the surface and the subsurface provides a fundamental control on water-energy fluxes and partitioning (*4*). Connections between the water table and evapotranspiration have been shown in model simulations (*5*–*9*) and observations of regional systems (*10*). Although theory to estimate and simulate evapotranspiration has evolved much over past decades (*11*), lateral groundwater flow has yet to be incorporated in continental-scale partitioning estimates (*12*). Quantifying the role of groundwater is important, because if partitioning is tied to water table depth and lateral flow, accurate predictions of future water availability will require a more detailed understanding of the underlying processes controlling groundwater surface water interactions than are currently included in most earth system simulators. Current research on partitioning relies on either isotope approaches or land surface models (*13*). These are fundamentally different methods, but both make critical assumptions about groundwater contributions to *T* and simplify groundwater surface water interactions. Discrepancies in partitioning estimates remain, and some have suggested that it may be systematically underestimated by current earth system models (*13*, *14*).

We used a continental-scale integrated hydrology model simulation to study the role that lateral groundwater flow plays in evapotranspiration partitioning (*15*). We used the ParFlow model (*16*, *17*), which couples groundwater and surface water flow with vegetation processes and snow dynamics (*7*, *18*) to solve a complete water and energy balance [figs. S1, S2, and S4 (*15*)]. The domain covers 6.3 million km^2 and encompasses major river basins in North America [including the Mississippi, Colorado, and Ohio basins; see Fig. 1 and fig. S3 (*15*)]. Simulations were run for one water year at hourly resolution driven by reconstructed meteorology. Transient simulations were initialized using the results of a prior steady-state model over the same domain (*19*) and additional transient model initialization [tables S1 and S2 (*15*)]. The model was compared to 1.2 million transient observations of stream flow, groundwater, and snow, and was shown to match observed behavior [figs. S5 to S20 (*15*)].

This simulation generated roughly 1.3 trillion outputs over the 1-year period, covering all key components of the water energy budget. Two variables that exemplify hydrologic stores and land-energy fluxes—water table depth and *LH* flux (the energy counterpart to *ET*)—show many scales of detail within these output fields (Fig. 1). For example, although groundwater is generally shallower in the more humid eastern region of the domain and deeper in arid western regions, laterally convergent flow drives local variability, creating shallow water tables in river valleys that can supply surface water export. We see similar patterns in *LH* flux, large-scale trends also driven by climate gradients, yet nested hillsllope-scale fluctuations persist.

The integrated model we used provides the ability to explicitly evaluate interactions between variables that are excluded from other global approaches (i.e., water table depth and individual land-energy flux components such as *T* and *E*). For example, the ratios of plant transpiration to total evapotranspiration (*T/ET*) are calculated directly from model outputs and compared to compiled stand-scale (*14*) and global (*4*, *20*, *21*) isotopically based partitioning estimates [Fig. 2, A and B (*15*)]. We see broad agreement between model simulations and estimates across scale; the domain-averaged *T/ET* of 62 ± 12% agrees with recent global isotope estimates (*4*, *14*, *20*, *21*).

To determine the role of lateral groundwater flow in these partitioning estimates, we performed a second simulation that is identical to the base case but allowed only vertical water movement, with no topographic influences or lateral flow. This approach is similar to current practice in land surface models (*15*). This "no lateral flow" simulation resulted in a domain-averaged *T/ET* of 47 ± 13%, suggesting that lateral groundwater flow plays a substantial role in the partitioning of evapotranspiration. This shift was seen systematically across all vegetation types, resulting in a lower prediction of stand and global scale estimates [fig. S20 (*15*)]. This indicates that topographically driven lateral flow provides an additional water source for transpiration in groundwater convergence zones.

To evaluate the relationships between partitioning and groundwater directly, we plotted the annual average *LH* flux, accumulated T and *E*, and *T/E* ratio against water table depth for nine tree and shrub land cover types, colored by soil type: more than 3.2 million points in total (Fig. 2, B to E). The distinct patterns shown in all four plots indicate a connection between water table depth and land-energy fluxes. Plots of *LH*, *T*, and *E* each follow logistic curves with three distinct regions: (i) an energy- or temperature-controlled region at shallow water table depths, where lateral groundwater flow stabilizes soil moisture and removes any water limitation; (ii) a deep disconnected groundwater region where surface fluxes are dependent on precipitation (i.e., water-limited); and (iii) a groundwater-controlled region discussed in prior modeling (*8*) and observational (*10*) studies, where land-energy fluxes are correlated with water table depth.

Similar to *T* and *E*, *T/E* ratios (Fig. 2F) also show a clear groundwater dependence; however, they do not follow the same logistic curve behavior as their composite fluxes. Here a maximum *T/E* partitioning [up to 35 in some locations, which also agrees with recent global isotopically derived estimates of *T/E* (*4*)] occurs at medium groundwater depths (0.5 to 5 m). We showed that this change in *T/E* is due to different depths to

[1]Integrated GroundWater Modeling Center, Department of Geology and Geological Engineering, Colorado School of Mines, Golden, CO, USA. [2]Department of Civil and Environmental Engineering, Syracuse University, Syracuse, NY, USA.

MS no: REaaf7891/CT/GEOCHEM PHYS

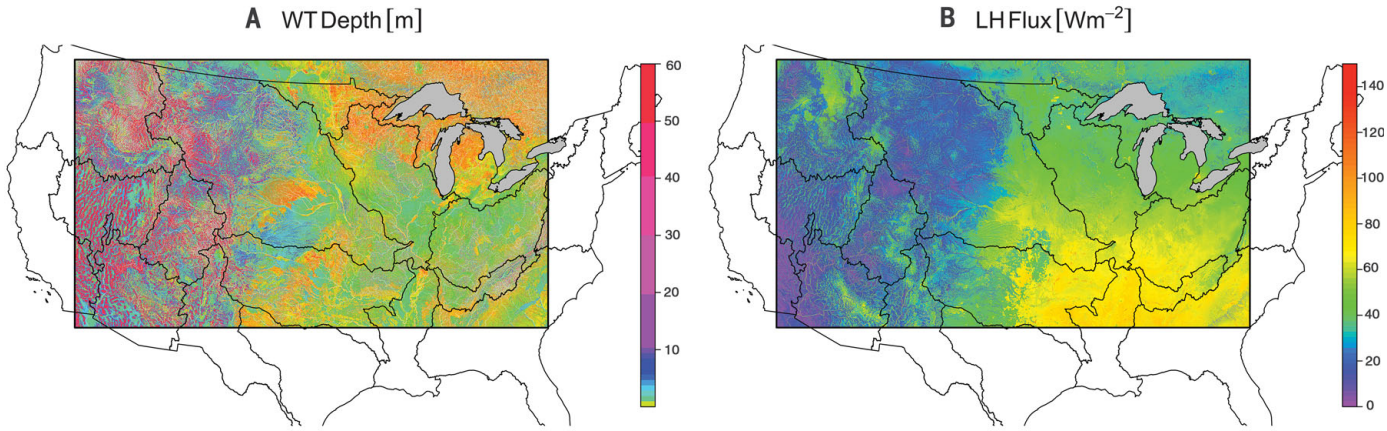

Fig. 1. Simulation results display great spatial complexity. Plots of transient (water year 1985) annually averaged water table (WT) depth (A) and *LH* flux (B) demonstrate the great detail we see in this simulation. Water table varies with climatic region; it is generally deeper west of the aridity divide and shallower in the east. Likewise, *LH* flux is also greater in less water-limited regions but exhibits larger values in river valleys, where the water table depths are locally shallow under what might otherwise be water-limited conditions.

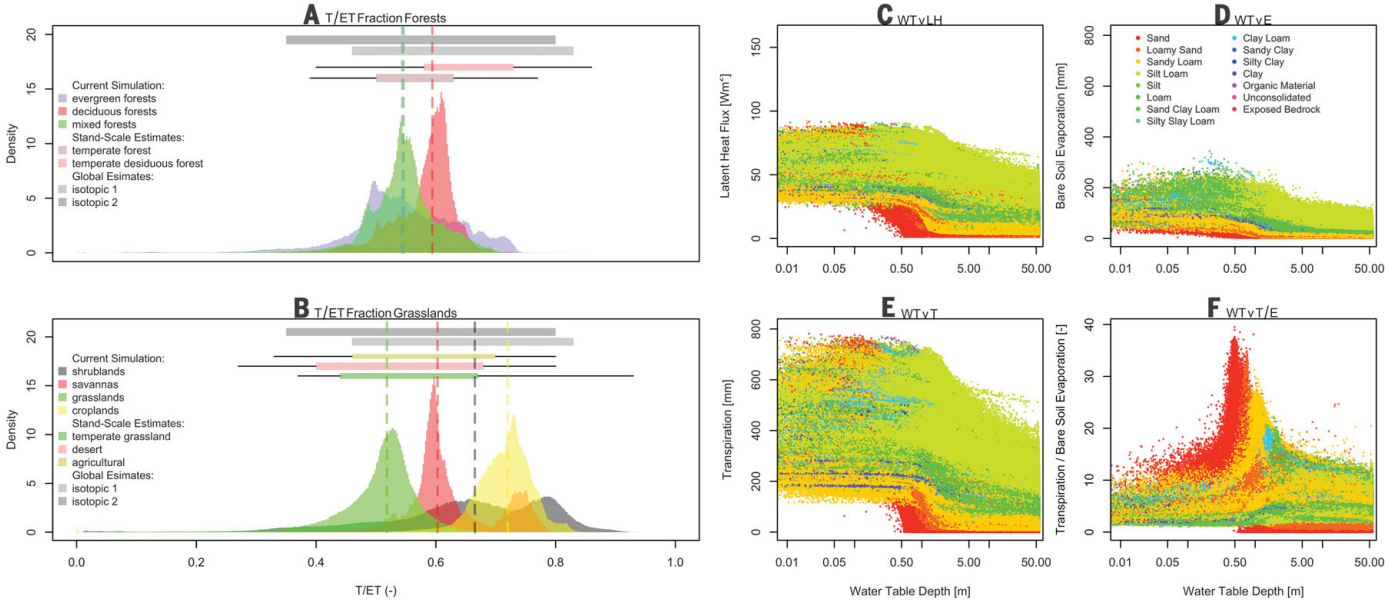

Fig. 2. Simulated annually averaged histograms of evapotranspiration partitioning compare favorably to observations and are related to water table depth. Simulated *T/ET* (–) xxxxxxxxx (**A** and **B**) plotted by land cover type agree with stand-scale estimates and observations (*14*) and are bracketed by global isotopic estimates, isotopic 1 (*4*) and isotopic 2 (*20*, *21*), shown here as box plots. Scatterplots of water table versus *LH* flux (**C**), bare soil evaporation (**D**), and *T* (**E**) suggest that groundwater's role in moderating these fluxes (*7*–*9*, *27*) extends across our continental-scale domain. When plotted as a function of water table depth, the *T/E* ratio (**F**) peaks at the middle of the groundwater critical depth, suggesting that *T* may be as much as 35 times greater than *E* because of lateral groundwater flow.

available water for the separate *E* and *T* processes. *E* interfaces at the shallow soil surface, whereas *T* draws water deeper from within the root zone (*15*). A simple conceptual hillslope model (Fig. 3) F3 shows that both *T* and *E* follow a similar logistic curve with respect to water table depth, but the depth range over which *E* is sensitive to water table depth is shallower than that for *T*. This shift creates a peak in *T/E* at groundwater depths where *E* is water-limited but *T* is not. This suggests that plants' access to deeper water allows them to draw water after the shallow soil is dry and can shift the balance of *T* partitioning in a manner not currently included in earth system models.

These results indicate that integrated simulations of the terrestrial hydrologic cycle can provide insights into process interactions that are currently lacking from other approaches, and they further motivate the need to advance model development as well as observations in this area. For example, although the 1-km resolution used for this simulation is fine-scale over such a large extent, there are always processes below the grid scale that might be better represented with increased resolution. Additionally, these simulations do not include any anthropogenic influences, such as groundwater pumping, irrigation, surface water diversions, reservoirs, and urbanization. We envision a road map where these assumptions are systematically relaxed and the model is continuously reevaluated against all available observations [fig. S6 (*15*)].

Although there has been much recent debate regarding *ET* partitioning, our results suggest that lateral groundwater flow processes currently overlooked in global approaches may play an important role in characterizing evapotranspiration at large scales. Our integrated hydrologic simulation

MS no: REaaf7891/CT/GEOCHEM PHYS

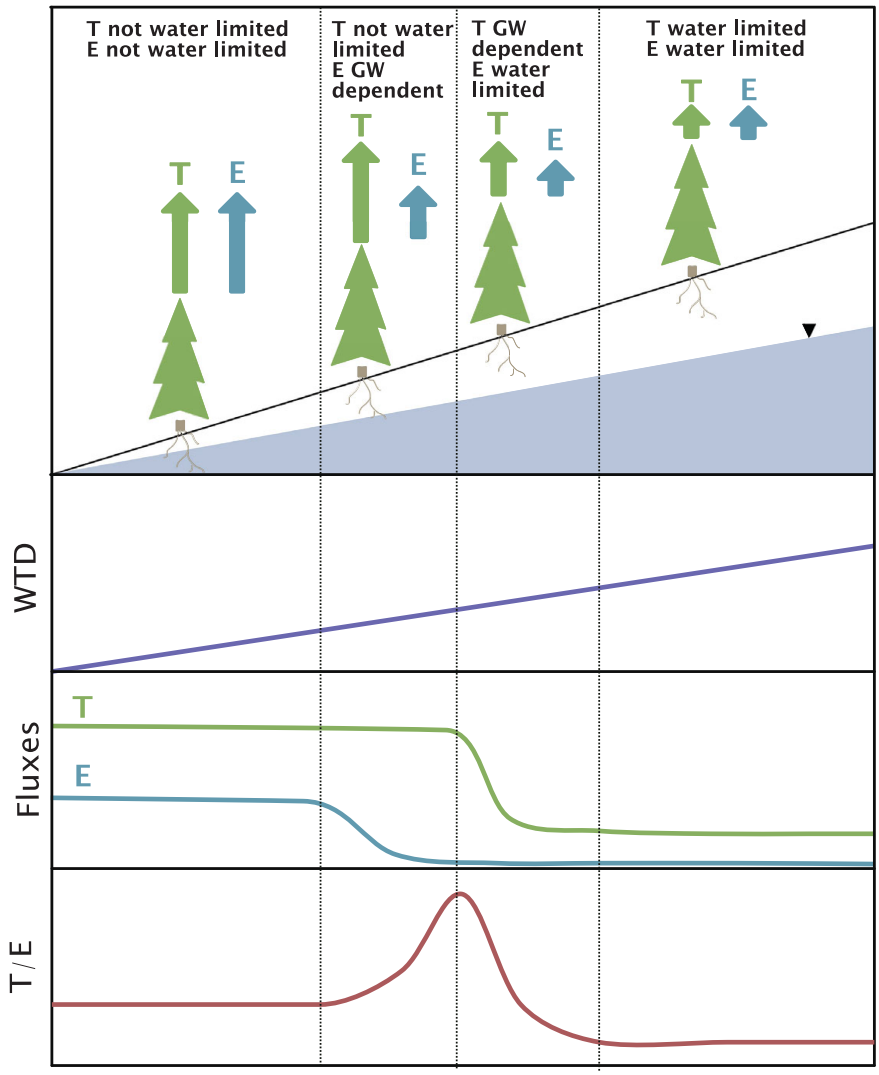

Fig. 3. The relationship between groundwater depth and land-energy fluxes for an idealized hillslope. On the left, groundwater (GW) is shallow and neither *T* or *E* is water–limited, because of lateral groundwater convergence, which stabilizes soil moisture. On the far right, groundwater is deep and disconnected from the land surface, resulting in lower *T* and *E* that are limited by precipitation. In the two center regions, *T* or *E* varies with groundwater depth, but *E* disconnects at shallower depths than *T*. As a result of these behaviors, *T/E* partitioning is sensitive to water table depth across both center regions. The peak in *T/E* reflects the differential in response to water table changes in *E* as compared to *T*. The roots as drawn here are not to scale and do not reflect potential changes in density due to water table depth, nor does this figure reflect the presence of subsurface heterogeneity.

over most of the major river basins in continental North America suggests that groundwater not only moderates *E* and *T* over the continent, but may also increase the partitioning of *T* substantially. This underscores the importance of including lateral groundwater flow and storage in earth system models (*22*), as well as developing careful multiscale observations of land surface fluxes and water table depth to better explore this relationship (*12*). Finally, the impact of groundwater on land-energy fluxes may have important implications for atmospheric simulation (*23*, *24*) and suggests that these feedbacks may go both ways: Changes in water table depth due to widespread worldwide pumping may have a profound influence on land-energy fluxes and climate (*25*, *26*).

REFERENCES AND NOTES

1. K. E. Trenberth, L. Smith, T. Qian, A. Dai, J. Fasullo, *J. Hydrometeorol.* **8**, 758–769 (2007).
2. K. E. Trenberth, J. T. Fasullo, J. Kiehl, *Bull. Am. Meteorol. Soc.* **90**, 311–323 (2009).
3. S. I. Seneviratne, D. Lüthi, M. Litschi, C. Schär, *Nature* **443**, 205–209 (2006).
4. S. P. Good, D. Noone, G. Bowen, *Science* **349**, 175–177 (2015).
5. J. S. Famiglietti, E. F. Wood, *Water Resour. Res.* **30**, 3061–3078 (1994).
6. G. D. Salvucci, D. Entekhabi, *Water Resour. Res.* **31**, 1725–1739 (1995).
7. S. J. Kollet, R. M. Maxwell, *Water Resour. Res.* **44**, W02402 (2008).
8. R. M. Maxwell, S. J. Kollet, *Nat. Geosci.* **1**, 665–669 (2008).
9. L. E. Condon, R. M. Maxwell, S. Gangopadhyay, *Adv. Water Resour.* **60**, 188–203 (2013).
10. J. Szilagyi, V. A. Zlotnik, J. Jozsa, *Ground Water* **51**, 945–951 (2013).
11. K. Wang, R. E. Dickinson, *Rev. Geophys.* **50**, XX–XX (2012).
12. P. D. Brooks *et al.*, *Water Resour. Res.* **51**, 6973–6987 (2015).
13. S. J. Sutanto *et al.*, *Hydrol. Earth Syst. Sci.* **18**, 2815–2827 (2014).
14. W. H. Schlesinger, S. Jasechko, *Agric. For. Meteorol.* **189–190**, 115–117 (2014).
15. Materials and methods are available as supplementary materials on *Science* Online.
16. S. J. Kollet, R. M. Maxwell, *Adv. Water Resour.* **29**, 945–958 (2006).
17. R. M. Maxwell, *Adv. Water Resour.* **53**, 109–117 (2013).
18. R. M. Maxwell, N. L. Miller, *J. Hydrometeorol.* **6**, 233–247 (2005).
19. R. M. Maxwell, L. E. Condon, S. J. Kollet, *Geosci. Model Dev.* **8**, 923–937 (2015).
20. S. Jasechko *et al.*, *Nature* **496**, 347–350 (2013).
21. A. M. J. Coenders-Gerrits *et al.*, *Nature* **506**, E1–E2 (2014).
22. M. P. Clark *et al.*, *Water Resour. Res.* **51**, 5929–5956 (2015).
23. R. M. Maxwell, F. K. Chow, S. J. Kollet, *Adv. Water Resour.* **30**, 2447–2466 (2007).
24. X. Jiang, G. Y. Niu, Z. L. Yang, *J. Geophys. Res.* **114**, D06109 (2009).
25. I. M. Ferguson, R. M. Maxwell, *Environ. Res. Lett.* **7**, 044022 (2012).
26. M. F. P. Bierkens, *Water Resour. Res.* **51**, 4923–4947 (2015).
27. J. F. Rihani, R. M. Maxwell, F. K. Chow, *Water Resour. Res.* **46**, W12523 (2010).

ACKNOWLEDGMENTS

This work was supported by the U.S. Department of Energy Office of Science, Offices of Advanced Scientific Computing Research and Biological and Environmental Sciences IDEAS project. All simulations were made possible through high-performance computing support from Yellowstone (ark:/85065/d7wd3xhc) provided by the National Center for Atmospheric Research's Computational and Information Systems Laboratory, sponsored by the National Science Foundation. The authors declare no financial conflicts. We thank M. M. Forrester for development and presentation of the graphics in figs. S1 and S6, L. Bearup for review comments, A. Bandler for assistance with surface water data processing, and D. Osei-Kuffuor for assistance with the analytical Jacobian. We also thank the anonymous reviewers for their constructive comments. All simulation data, models, and inputs are archived and are available. Specific versions of ParFlow are archived with complete documentation and may be downloaded at (http://inside.mines.edu/~rmaxwell/maxwell_software.shtml) or checked out from a commercially hosted, free SVN repository and GITHUB; r730 was the version used in this study. The input data and simulations presented here are available as supplementary materials on *Science* Online. R.M.M. and L.E.C. designed the study and prepared the input data; R.M.M. ran the numerical experiments; L.E.C. developed the model-observation comparison framework and metrics; and R.M.M. and L.E.C. synthesized the results, made the figures, and wrote the manuscript.

SUPPLEMENTARY MATERIALS

www.sciencemag.org/content/[volume]/[issue]/[page]/suppl/DC1
Materials and Methods
Supplementary Text
Figs. S1 to S20
Tables S1 and S2
References (*28–68*)
Table S1 (Model Input)
Table S2 (Model Output)

30 March 2016; accepted 22 June 2016
10.1126/science.aaf7891